Acidic and adsorptive properties of SBA-15 modified by aluminum incorporation

Brindusa Dragoi, Emil Dumitriu, Claude Guimon, Aline Auroux

Acidic and adsorptive properties of SBA-15 modified by aluminum incorporation

B. Dragoi [a,b], E. Dumitriu [b], C. Guimon [c], A. Auroux [a,*]

[a] *Institut de Recherches sur la Catalyse et l'Environnement de Lyon, UMR 5256, CNRS – Université Lyon I, 2 Av. Einstein, 69626 Villeurbanne, France*
[b] *Laboratory of Catalysis, Faculty of Chemical Engineering and Environmental Protection, Technical University, 71 A Mangeron Av., 700050 Iasi, Romania*
[c] *L.C.T.P.C.M., UMR 5624, Université de Pau et des Pays de L'Adour, 2 Av. P. Angot, 64053 Pau Cedex 9, France*

In this work, Al-SBA-15 samples with different Si/Al ratios were synthesized; Al was incorporated in the mesoporous SBA-15 structure either using the direct synthesis method, with tri-block copolymer P123 as surfactant, or by the post-synthesis method. The porous solids were characterized using different tech-niques, such as: XRD, pore size distribution, ^{27}Al MAS NMR, and XPS. Acidic properties were estimated by adsorption and titration microcalorimetry, respectively. Ammonia and pyridine were used as probe mol-ecules in the first case, while aniline in n-decane was used in the second one. FT-IR of pyridine adsorption and XPS of ammonia adsorption completed the characterization of acid properties. The increase of acidity with the incorporation of aluminum was evidenced; lower Si/Al ratios led to higher acidity of the sample. Microcalorimetry was also used to test the adsorption properties of these mesoporous materials toward pollutants such as methyl ethyl ketone, propionaldehyde and acetonitrile (in gas phase) and nicotine (in aqueous phase). The ketone was better retained in comparison to the other two molecules. Regarding nicotine, its adsorption was strongly influenced by the aluminum content in the solids; the higher the quantity of aluminum, the lower the adsorption of nicotine.

1. Introduction

Microporous zeolites with regular arrays of uniformly sized channels have been widely used for many purposes including adsorption, separation, ion exchange and catalysis for many years [1]. However, their relatively small pores (with a diameter usually less than 2 nm) cannot admit large molecules, leading to the limitation of their applications. The synthesis of mesoporous MCM-41 materials by Mobil researchers [2] in 1992 with pore size in the range of 1.5–10 nm satisfied the size requirements, but their relatively low hydrothermal stability and weak acidity would limit their practical applications. In 1998, Zhao et al. [3] synthesized a new type of mesoporous material with uniform two-dimensional hexagonal structure, named SBA-15, by using neutral polymeric surfactants (e.g., Pluronic 123) as templating agents. Compared with microporous zeolites, this material is characterized by larger pore sizes, up to approximately 30 nm, and allows bulky molecules to enter into the pores. At the same time, it has higher hydrothermal stability and thicker pore walls (3.1–6.4 nm) compared to mesoporous MCM-41 materials. For these reasons, the discovery of SBA-15 provided a potential for designing new materials, applicable as catalysts and adsorbents for bulkier molecules. On the other hand, the purely siliceous SBA-15 materials have only silanol groups on their surface, which are of low acid strength and catalytically non-active. Therefore, in order to make these materials useful for catalysis, stronger acidic sites have to be introduced into their framework. Generally, the substitution of heteroatoms with valence lower than silicon creates negative charges in the framework which can be compensated by protons, thus generating acidity in these materials. Concerning mesoporous materials containing aluminum, Trombetta et al. [4] argued that the Brönsted acid sites result from terminal silanol groups in the vicinity of an aluminum atom, so-called bridging hydroxyl groups, as illustrated in Fig. 1.

Two methods have been developed in order to incorporate aluminum atoms into the framework of mesoporous materials: direct synthesis [5,6] and post-synthesis [7–9]. The direct synthesis is difficult to perform because of the dissociation of the metal–O–Si bond in acid media as well as the high difference in the hydrolysis rates between silicon alkoxides and aluminum alkoxides; thus it is a challenge to directly synthesize Al-substituted SBA-15 materials through a standard hydrothermal method [10]. The incorporation of aluminum in SBA-15 follows the same mechanism as for pure SBA-15, namely through $(S^0H^+)(X^-I^+)$ where (S^0H^+) = nonionic polymeric surfactant, X^- = halogen anions, and I^+ = the protonated inorganic SiO_2 species [5,11]. Post-synthesis alumination in aqueous solution was developed by Mokaya and Jones [12,13] on pure silica MCM-41 support. The post-synthesis method could be considered as a strategy for improving the amount of aluminum

* Corresponding author.
E-mail address: aline.auroux@ircelyon.univ-lyon1.fr (A. Auroux).

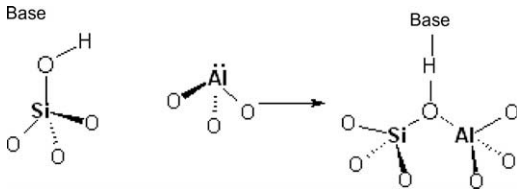

Fig. 1. Formation of terminal Brönsted acidic OH groups in mesoporous materials.

incorporated in the sample. This method leads to a fairly high amount of EFAL aluminum, but the amount of tetrahedral aluminum is nonetheless higher than in the case of direct synthesis.

The aim of this work was to perform a detailed characterization of the structural and acidic properties of Al-containing mesoporous materials obtained by both methods, as well as to investigate their relationship with the adsorption performance in the retention of four organic compounds namely propionaldehyde or propanal, methyl ethyl ketone or 2-butanone, acetonitrile or ethanenitrile, and nicotine, belonging to the VOC class of pollutants.

2. Experimental

2.1. Materials and synthesis

Purely siliceous SBA-15 was synthesized following a previously published method [3]. Aluminum incorporation into the SBA-15 lattice was performed either by direct synthesis [14], using a slightly improved procedure, or post-synthesis [7,8]. Modified SBA-15 samples were denoted as Al-SBA-15. The precursors were: tetraethylorthosilicate ($Si(OC_2H_5)_4$,TEOS, 98%, Aldrich) as silica source, aluminum *iso*-propoxide ($Al[OCH(CH_3)_2]_3$, 98%, Aldrich) and aluminum hexachloride ($AlCl_3 \cdot 6H_2O$, 99%, Aldrich) as aluminum sources, non-ionic triblock co-polymer Pluronic P123 (poly(ethylene oxide)-*block*-(poly(propylene oxide)-*block*-poly (ethylene oxide), $EO_{20}PO_{70}EO_{20}$, molecular weight = 5800, BASF Corp.) as template, tetramethylammonium hydroxide ($(CH_3)_4NOH$, TMAOH 10%, Aldrich), distilled water and hydrochloric acid.

Adsorption capacity experiments were performed using propionaldehyde (C_2H_5CHO, 98%, Merck), methyl ethyl ketone ($CH_3COC_2H_5$, 99%, Merck), acetonitrile (CH_3CN, 99%, Merck), and nicotine ($C_{10}H_{14}N_2$, 99%, Fluka).

2.1.1. Synthesis of SBA-15 and Al-SBA-15 by direct-synthesis method

In a typical synthesis of SBA-15, 4 g of Pluronic P123, water and HCl 0.28 M were stirred at 35 °C for 16 h. The appropriate amount (8.5 g) of TEOS was then added dropwise to the surfactant solution, followed by stirring for 24 h. The resulting gel was introduced into a Teflon-lined stainless steel autoclave and heated at 100 °C for two days.

Al-SBA-15 was prepared as follows. The required amounts of aluminum *iso*-propoxide necessary to get the desired Si/Al ratio, distilled water, TEOS (9 g) and hydrochloric acid (0.28 M) were stirred at 35 °C. After a clear solution was obtained, Pluronic P123 was added and the mixture was stirred for another three days at 35 °C. The hydrothermal treatment was carried out in a Teflon-lined stainless steel autoclave at 100 °C for 24 h. All the samples obtained by direct and post-synthesis were washed with distilled water and dried at 80 °C overnight. The open pore structure was obtained by removing the surfactant by calcination in air flow at 500 °C for 6 h with a heating rate of 2.5 °C min^{-1}. Synthesized Al-SBA-15 samples were denoted as Al-SBA-15 ($Si/Al_{gel} = n$) where n represents the Si/Al ratio in the gel.

2.1.2. Synthesis of Al-SBA-15 by post-synthesis method

10 ml of aqueous solution of $AlCl_3 \cdot 6H_2O$ (the molar concentration of the solution was depending on the required amount of aluminum) and the appropriate amount of TMAOH 10% (TMAOH/Al molar ratio = 2) were heated under stirring at 70 °C. After a clear solution was obtained, 1 g of pure SBA-15 was added under stirring. The mixture was stirred for 2 h at the same temperature. After filtration, washing and drying at 80 °C, the product was calcined at 500 °C for 3 h in air flow with a heating rate of 2.5 °C min^{-1}. Synthesized Al-SBA-15 samples were denoted as Al-SBA-15ps ($Si/Al_{gel} = n$) where n represents the Si/Al ratio in the gel.

2.2. Characterization

X-ray powder diffraction patterns were recorded on a Bruker D5005 diffractometer using a monochromatized CuK_α radiation ($\lambda = 0.154$ nm) in the angular range from 0.5 to 10° (2θ) with a scanning rate of 0.002° (2θ)/s.

Nitrogen physisorption measurements were carried out at −196 °C on an ASAP 2010 Micromeritics apparatus. The isotherms were used to quantify the textural properties of the samples. The specific surface areas (S_{BET}) of the samples were calculated using the BET method in the standard pressure range 0.05–0.3 p/p°. The total pore volume V_p was evaluated on the basis of the amount adsorbed at a relative pressure of about 0.98, by converting the amount of nitrogen gas adsorbed at STP to the liquid volume at −196 °C (using the conversion factor $c = 0.001547$). The pore size distributions were obtained from the desorption branch of the isotherm using the corrected form of the Kelvin equation by means of the Barrett–Joyner–Halenda method with a cylindrical pore model. The external surface area (S_{ext}) and the micropore volume ($V_{\mu p}$) were assessed by the *t*-plot method, using the Harkins-Jura equation to estimate the thickness of a monolayer of nitrogen adsorbed at −196 °C, t ($t = [13.99/(0.034\text{-log } p/p°]^{1/2}$.

The amount of aluminum present in the samples was determined by *chemical analysis* using inductively coupled plasma emission spectroscopy (ICP-ES). For that purpose, the samples were treated with a mixture of $HCl + HF + HNO_3$ in order to dissolve them completely.

XPS experiments for surface composition determination were carried out on a VG Scientific ESCALAB 200R spectrometer including a hemispherical analyzer and working at a pressure lower than 10^{-7} Pa. The measurements were performed using the Al Kα line of the dual anode and a pass energy of 50 eV. The peaks were referenced to the C-(C, H) components of the C1s band at 284.6 eV. The XPS experiments for ammonia adsorption were performed on a SSI 301 spectrometer using a monochromatic and focused AlK_α radiation under a residual pressure of 10^{-7} Pa. Ammonia was adsorbed at 80 °C on the calcined samples and then outgassed under helium at 350 °C. The proportion of each type of site was evaluated by analyzing the N1s band.

Infrared spectra were recorded on a Bruker Vector-22. Samples were used as self-supported wafers (around 10 mg) obtained under 1000 kg m^{-2} pressure. The wafers were calcined overnight under O_2 in the IR cell at 400 °C and then evacuated under vacuum for 2 h. After cooling down to room temperature and adsorption of pyridine, the cell was evacuated for 20 min at several temperatures (25, 100, 200, 300, 400 °C). A spectrum was collected for each stage at room temperature.

The state of the aluminum in the SBA-15 lattice was investigated by ^{27}*Al MAS NMR spectroscopy*. After hydration of the samples for two nights in a desiccator, the spectra were recorded at 104.27 MHz on a Bruker DSX 400 spectrometer.

Gas phase adsorption microcalorimetry. The experiments were carried out in a microcalorimeter of Tian–Calvet type (C80 from Setaram) linked to a volumetric line. NH_3 and pyridine were chosen as base probe molecules for characterizing the acidic properties. The adsorption capacities of the mesoporous samples for organic molecules were evaluated by choosing four test molecules

which belong to four different categories of organic derivatives, namely: acetonitrile (nitriles), propionaldehyde (aldehydes), methyl ethyl ketone (ketones) and nicotine (alkaloids with two nitrogen atoms). These organic molecules are among the most frequently encountered pollutants in both air and water. The solids were pretreated under vacuum at 350 °C overnight. The adsorption experiments consisted in repeatedly sending small doses of gas onto the solid while the heat flow signal and the concomitant pressure evolution were recorded (until an equilibrium pressure of 67 Pa was reached). The adsorptions were carried out at 30, 80 and 150 °C for VOCs, NH_3 and pyridine, respectively. A readsorption was performed after outgassing the samples for 0.5 h at the same temperatures in order to determine the chemisorbed uptake (V_{irr}).

Titration microcalorimetry. The adsorption heats of aniline (C_6H_7N, 99.5%, Aldrich) diluted in n-decane ($C_{10}H_{22}$, 99%, Sigma) and of nicotine ($C_{10}H_{14}N_2$, 99%, Fluka) dissolved in water were measured in a differential heat flow reaction calorimeter equipped with a stirring system (TITRYS, from Setaram). Using a syringe pump, successive pulse injections of known amounts of a solution (0.03 M) of the probe molecule were sent onto the sample maintained at 35 °C at 2 h time intervals. A preheating furnace allowed the injection of the solution at the same temperature as the calorimeter. The reference and measurement cells contained the pure solvent (1.5 ml) and the solvent with a weighted amount of the outgassed solid sample (ca. 150 mg), respectively. A programmable syringe pump (PH 2000, Harvard Apparatus) was linked to the calorimeter by capillary tubes. The samples were pretreated under vacuum at 350 °C for 4 h before being transferred into the calorimeter cell. Each dose was accompanied by an exothermic peak. The evolved heat was evaluated by the SETSOFT acquisition and processing software from SETARAM and represented as a function of the probe amount injected.

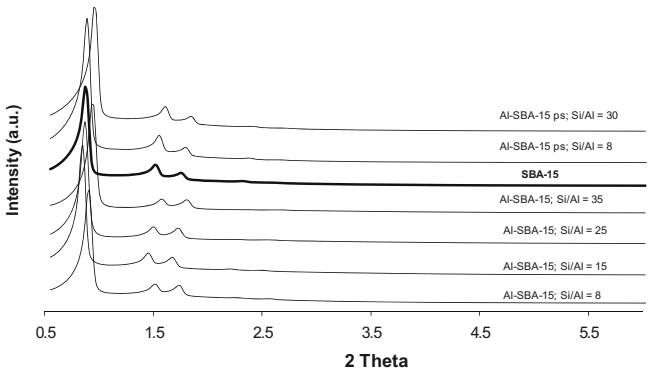

Fig. 2. XRD patterns of studied samples.

3. Results and discussion

3.1. Materials characterization

Using triblock copolymer P123 as organic directing agent under acidic conditions, SBA-15 and Al-SBA-15 with different Si/Al ratios and ordered two-dimensional hexagonal (*P*6mm) mesostructure and thick uniform silica walls (16–62 Å) were obtained (Fig. 2 and Table 1).

The small angle XRD patterns (Fig. 2) show three different peaks that can be indexed as (100), (110) and (200) reflections. The most important peak (100) reflects a large d_{100} spacing (91–103 Å) corresponding to a large lattice parameter (a_o = 105–119 Å). All the diffraction patterns suggest the preservation of the SBA-15 structure after incorporation of Al either by direct or post-synthesis methods. Anyway, only a slight broadening of the (110) reflection peaks for the Al-SBA-15 obtained by direct synthesis can be observed, as well as a slight shifting of the (100) peak to higher 2θ values and a lower *d*-spacing after Al incorporation either by direct synthesis or grafting. The same behavior has been reported for Al-MCM-41 obtained by grafting [15], Al-SBA-15 obtained by grafting [16] and Al-MCM-41 obtained by direct synthesis [17]. This behavior might possibly be caused by a slight distortion of the mesoporous channels or pore narrowing due to the deposition of the Al clusters on the inner pore walls.

Analysis of the N_2 sorption isotherms (Table 1 and Supplementary material 1) indicates that all samples are predominantly mesoporous solids although some amounts of intrawall pores can be found in all samples. Surface areas found for our samples range from 522 to 993 $m^2\,g^{-1}$, while pore volumes vary between 0.96 and 1.44 $cm^3\,g^{-1}$. Moreover, an increasing of the S_{BET} of pore volumes as compared to pure SBA-15 was noticed when aluminum was introduced by direct synthesis while grafting led to a decreasing of these parameters. Compared to MCM-41, the ordered mesoporous silica SBA-15 has an additional system of secondary mesopores (around 20 Å) and micropores, which intersect the regular structure of parallel mesopores [18–21]. Though this additional microporous system facilitates the diffusion of small molecules, often it also exhibits a "pore blocking effect" [22]. This pore blocking effect leads to a delayed capillary evaporation and renders the relation between the capillary evaporation pressure and the pore size ambiguous [23]. Moreover, the post-synthesis method could induce a partial degradation of the pore structure by alkaline dissociation, since the alumination was performed in basic media. This could explain the reduction in the surface area and pore volume of the Al-SBA-15 samples obtained by grafting, as well.

As mentioned above, aluminum incorporation by direct synthesis led to an increase in total surface area and in micropore volume compared to purely siliceous SBA-15. As a general trend, the values

Table 1
Structural properties of samples.

Sample	Si/Al			XRD analysis		N_2 adsorption–desorption isotherm				
	gel	C.A.	XPS	d_{100} (Å)	a_0 (Å)	S_{BET} ($m^2\,g^{-1}$)	S_{ext} ($m^2\,g^{-1}$)	V_p ($cm^3\,g^{-1}$)	$V_{\mu p}$ ($cm^3\,g^{-1}$)	D_p (Å)
Al-SBA-15	8	26.5	27.2	98	113	840	91	1.33	0.037	63
Al-SBA-15	15	254.2	–	102	117	948	89	1.44	0.076	61
Al-SBA-15	25	307.5	–	100	115	993	65	1.33	0.11	53
Al-SBA-15	35	307.5	–	91	105	991	67	1.23	0.12	50
SBA-15	**–**	**–**	**–**	**103**	**119**	**721**	**38**	**1.18**	**0.046**	**65**
Al-SBA-15ps	8	2.7	13.5	–	–	522	34	0.96	0.012	66
Al-SBA-15ps	30	13.4	27.3	92	106	657	40	1.13	0.043	68

Bold corresponds to the reference sample.
Lattice parameter, a_o: $a_0 = \frac{2d_{100}}{\sqrt{3}}$; ps = post-synthesis; C.A. = chemical analysis, S_{ext} = external surface, V_p = total pore volume, $V_{\mu p}$ = micropore volume, D_p = average pore diameter.

of these parameters decrease as the aluminum content increases. These findings suggest an important contribution of the micropores and secondary mesopores. If the formation of micropores is due to the penetration of the hydrophilic poly(ethylene oxide) chains of the Pluronic P123 in the silica walls [16], then it could be considered that the presence of Al would facilitate this penetration and thus the formation of micropores is favored. For the sample with high Al content (labeled Al-SBA-15; $Si/Al_{gel} = 8$), the surface area, total pore and micropore volumes are decreased in comparison with the samples prepared by direct synthesis. This trend is in good agreement with the results of Ooi et al. [24], who found that too high an aluminum loading stimulates the deterioration of pore structure. However, the XRD pattern for our sample indicates a hexagonal arrangement of the pores. In this case, a narrowing of the pores due to the presence of non-framework aluminum could explain the decrease of the surface area and pore volume. It could be supposed that the micropores and secondary mesopores of this sample are most probably blocked by this EFAL aluminum.

The examination of the results obtained by chemical analysis (Table 1) shows an increase of the Si/Al ratio in the final product for the samples synthesized by direct-synthesis method, while for the samples obtained by post-synthesis, this ratio is much lower than in the synthesis gel. This finding was observed in previous studies, as well [5]. Thus, for the direct synthesis, it seems that the solubility of the aluminum iso-propoxide used as aluminum source in the acidic medium allows only statistical replacement of Si by Al, leading to higher Si/Al ratio. Of course, the possibility of losing part of the extra framework aluminum during the washing of the solid at the end of synthesis should also be taken into account. On the other hand, post synthesis incorporation of Al takes place in a basic medium (pH around 9), and lower silica to alumina ratios could be explained by partial alkaline extraction of silicon from the framework [7].

The ^{27}Al NMR analysis was performed only for the samples with the highest aluminum contents. For the other samples, it seems that the small amounts of aluminum which were introduced in the samples (see chemical analysis results in Table 1) probably exist as so-called "NMR invisible" ^{27}Al [14]. All recorded spectra show aluminum in two different coordination states corresponding to two different resonances as illustrated in Fig. 3.

For the three samples, the most important peak is around 50 ppm which is typical for tetrahedrally coordinated AlO_4 groups. The presence of extra framework six fold coordinated AlO_6 octahedra is indicated by a resonance near 0 ppm [25]. The sample denoted by *b* in Fig. 3, obtained by post-synthesis ($Si/Al_{gel} = 30$), exhibits a single resonance indicating that almost all aluminum atoms are in tetrahedral coordination (Table 1).

The acid character created by aluminum incorporation was evaluated using gas phase adsorption microcalorimetry. Ammonia ($pK_a = 9.24$, proton affinity in gas-phase = 857.7 kJ mol^{-1}, kinetic diameter = 0.375 nm) and pyridine ($pK_a = 5.19$, proton affinity in gas-phase = 922.2 kJ mol^{-1}, kinetic diameter = 0.533 nm) were chosen to probe the overall acidity of the solids, since both Lewis and Brönsted acid sites retain these molecules. Generally, the heat evolved during the adsorption of a molecule on a solid surface at constant temperature is known as the differential heat of adsorption ($Q_{diff} = \partial Q_{int}/\partial n_a$) and it is graphically represented as a function of the surface coverage (n_a). It is claimed that the heat evolved during the adsorption of a basic molecule on an acidic site reflects the acid strength of this site. Moreover, the dependence of the heat of adsorption on coverage provides information about the heterogeneity of the acid strength. For this purpose, the temperature of adsorption has to be high enough to ensure that the probe molecule reaches the sorption equilibrium on the sites of interest. The temperature of the pretreatment is also very important, since it

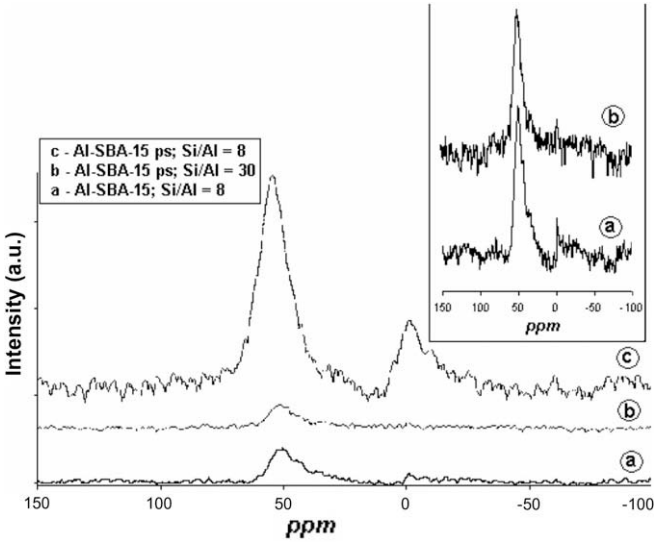

Fig. 3. ^{27}Al MAS NMR spectra of three Al-SBA-15 samples; Al-SBA-15 ($Si/Al_{gel} = 8$); Al-SBA-15 ps ($Si/Al_{gel} = 30$); Al-SBA-15ps ($Si/Al_{gel} = 8$).

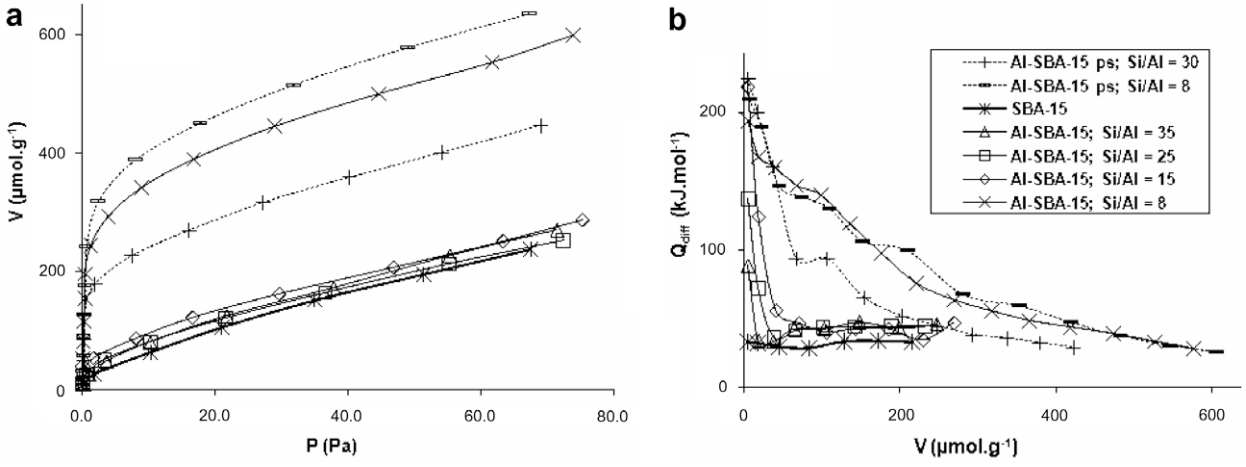

Fig. 4. Volumetric isotherms (a) and differential heats (b) of NH_3 adsorption at 80 °C for all studied samples.

can affect the surface acidity of the samples and thus the heat spectrum [26]. A typical differential heat plot shows different regions [27]. The first region corresponding to a sharp decrease of Q_{diff} at low coverage represents the adsorption on the strongest sites. Usually, these sites are attributed to Lewis sites. The next region of the curve is attributed to the interactions of probe molecules with sites of intermediate strength, which are predominantly of Brönsted type. When this part forms a plateau, it is an indicator of the homogeneity of the acid strength, while heterogeneity is reflected by a continuous decrease of the heat *vs*. coverage. At high uptake, the heat of adsorption is almost constant, which is characteristic to hydrogen bonds between the probe and the sample or physisorption of the probe. Differential heats of adsorption are presented in Fig. 4b, which plots the heat evolved for each dose *vs*. adsorbed NH_3 amount for Al-SBA-15 prepared by direct and post-synthesis, respectively.

The results obtained for Al-substituted SBA-15 can be compared with those for purely siliceous SBA-15. The heat evolved for SBA-15 is almost insignificant, around 30 kJ mol^{-1}, indicating that no acid sites of noteworthy strength are present in this sample. In accordance with the amount of aluminum present in the sample, and thus with the existence of acid sites, the heat evolved increases with decreasing of Si/Al ratio. Calorimetric curves for the samples with Si/Al_{gel} = 35, 25 and 15 indicate the existence of only a few Lewis sites on which NH_3 is firstly adsorbed. After that, the heat evolved is almost similar to that measured for SBA-15. Brönsted sites are more evident in the sample with Si/Al_{gel} = 8. After the strong Lewis sites are covered, the subsequent region of the heat curve presents a slow and continuous decrease until around 150 kJ mol^{-1}. Then a continuous decrease of the heats is observed until the physisorption region is reached; this also indicates the heterogeneity of the acid strength distribution. Calorimetric curves obtained for samples prepared by post-synthesis show the existence of Brönsted type sites, as well. Moreover, it seems that although the ^{27}Al NMR spectra show higher incorporation of Al in the post-synthesis sample with Si/Al_{gel} = 8, the strength of the acid sites is similar to that of the sample with the same Si/Al ratio but prepared by direct-synthesis.

The volumetric isotherms (number of adsorbed molecules, *n*, as a function of the equilibrium pressure, *p*) presented in Fig. 4a consist of two distinct parts.

The vertical part can be assigned to irreversible adsorption, namely chemisorption, while the horizontal part corresponds to reversible adsorption (physisorption). Of course, the samples with higher amounts of acid sites present more chemisorption than the samples containing a small amount of acid sites.

It is known that in the case of molecules larger than ammonia, the initial heats are only a statistical average of the sites which are firstly exposed. For this reason, it is recommended to increase the mobility of these kinds of molecules by increasing the adsorption temperature. As a consequence, pyridine adsorption was performed at 150 °C. Experiments carried out for post-synthesis samples and two of the direct-synthesis samples (Fig. 5) confirm the results obtained by ammonia adsorption. However, for the sample Al-SBA-15, Si/Al_{gel} = 8, prepared by post-synthesis, there is a plateau of adsorption heats at low coverage, usually attributed to an energetic homogeneity of the adsorption sites. It seems that in this case, pyridine is adsorbed on sites of similar strength. It is worth emphasizing here that the acidic properties of the two types of solids (i.e., samples obtained by direct synthesis and by grafting) are influenced by the nature of the aluminum precursor as well as by the method of aluminum incorporation. As it can be seen, the heat evolved for pyridine adsorption is higher than for ammonia adsorption. This difference was explained by Lee et al. [28] based on the gas phase affinity of these two probes. Another supplementary explanation is the way in which probe molecules bind on the solid surface. Thus, it was proven for zeolites H-ZSM-5 and H-MOR that pyridine forms a monodentate complex adsorbed on the surface, because the pyridinium ion only has a single proton available for H-bonding, while ammonium binds with two sites forming a bidentate complex [27,28]. Of course, the presence of the aromatic ring in the pyridine molecule has to be taken into consideration, as well. The electronic effects from the aromatic ring favor three cationic positions on the ring which are able to interact with the negative charges of the silica surface. These interactions could also explain the higher adsorption heats of pyridine compared to ammonia.

Table 2 summarizes the acidity measurement results obtained by adsorption calorimetry at 80 °C for NH_3 and 150 °C for pyridine, respectively. The total number of acid sites (in μmol probe per gram of sample) at the given equilibrium pressure of 27 Pa, the number of strong acid sites (derived from the irreversibly adsorbed probe volume), the integral heat at 27 Pa (in J g^{-1}), and the average differential heat (integral heat divided by probe uptake) over the 0–27 Pa range are listed.

Fig. 6 presents the heat evolved for each dose of diluted aniline as a function of the amount of probe sent on the samples dispersed in n-decane at 35 °C. The concerned samples are those which have the highest aluminum content: Al-SBA-15 obtained by post-synthesis, and two samples obtained by direct-synthesis, namely Al-SBA-15 (Si/Al_{gel} = 8 and 15). The results are compared to the evolved heat for aniline sent on purely siliceous SBA-15.

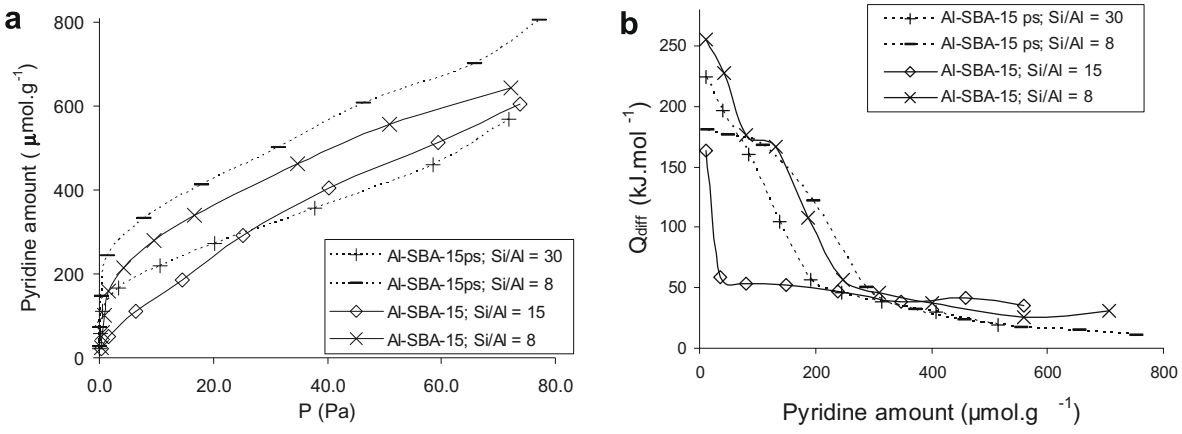

Fig. 5. Volumetric isotherms (a) and differential heats (b) of pyridine adsorption at 150 °C for samples obtained by post-synthesis and two samples obtained by direct-synthesis.

Table 2
Acidic properties of samples based on ammonia adsorption at 80 °C and pyridine adsorption at 150 °C, respectively.

Solid	Total number of acid sites (μmol g^{-1})[a]		Number of strong acid sites (μmol g^{-1})[b]		Integral heat (J g^{-1}) [c]		Average heat (kJ mol^{-1})[d]	
	NH_3	Py	NH_3	Py	NH_3	Py	NH_3	Py
Al-SBA-15 (Si/Al = 8)[e]	435	408	246	260	40	46	88	107
Al-SBA-15(Si/Al = 15)[e]	153	302	56	121	10	18	57	58
Al-SBA-15(Si/Al = 25)[e]	135	–	36	–	7	–	47	–
Al-SBA-15 (Si/Al = 35)[e]	139	–	36	–	6	–	39	–
SBA-15	**124**	**–**	**33**	**–**	**4**	**–**	25	–
Al-SBA-15 ps (Si/Al = 8)[e]	491	470	263	301	45	46	89	94
Al-SBA-15 ps (Si/Al = 30)[e]	314	303	314	204	26	33	78	105

[a] Adsorbed amount under an equilibrium pressure of 27 Pa.
[b] Number of strong acid sites obtained by difference between the adsorption and readsorption isotherms (V_{irr}).
[c] Integral heat of adsorption corresponding to an equilibrium pressure of 27 Pa.
[d] Integral heat divided by probe uptake.
[e] Molar ratio in gel.

To our knowledge, until now the surface acidity of Al-SBA-15 has not been investigated by calorimetry in liquid phase. In fact, even in the broader context of solid acid catalysts, there is only a limited amount of literature reporting calorimetric measurements of the reaction of bases with solid acids slurried in non-basic solvents [29]. Contrary to gas phase, in liquid media the adsorption is accompanied by complex phenomena. In this case, the active sites are covered by liquid which first of all has to be removed before the molecules to be adsorbed are retained by the solid. Depending on the strength of the acid sites, some of them could react with the solvent, thus preventing activity of these sites towards the probe. On the other hand, the solvent nature has a great influence on the strength of the acidic or adsorption sites of the solid [30]. The molecular interactions which can take place in the liquid phase are as follows: solvent–solid, solvent–solvent; solvent–probe molecule, solid–probe molecule, and probe molecule–probe molecule. As it will be seen below, these complex relationships all participate in determining the acidity of a solid in liquid phase. Knowledge of the behavior of the solid in liquid media provides key information for finding the most appropriate solid–solvent–probe molecule triad when the maximum catalytic performance of the solid is desired. Moreover, the combination of adsorption gas phase microcalorimetry with titration microcalorimetry gives more complete and realistic information about the acidity of the solid.

The evolved heats for the first injected doses were between 6 and 2 J g^{-1}. The next doses found a surface partly occupied by the probe and therefore a smaller number of molecules were adsorbed, leading to the decreasing of the evolved heat. For our samples, the heat of adsorption gradually diminished to values of 1.5–0.3 J g^{-1}. A general analysis of the curves shows a reversed acidity scale compared to gas phase experiments (see Figs. 4 and 5), except for SBA-15 which manifests the lowest acidity in both media. First of all, it could be supposed that, due to the competition between solvent and probe, in liquid phase the active sites are not occupied depending on their acid strength but rather depending on their ability to liberate the solvent. The evolved heats measured upon aniline adsorption are in fact the sums of the contributions of two effects: the exothermic enthalpy of neutralization of the acid site, ΔH_{neut} and the endothermic enthalpy of the solvent displacement, ΔH_{dpl}, respectively. Regarding the thermal effects due to other phenomena such as stirring, dispersion, dilution and solvation by decane, these are compensated by the reference cell, which contains the solvent only [30,31]. Moreover, the exothermic enthalpy of neutralization, ΔH_{neut}, represents a sum of different contributions, as well: the loss of one proton by the acid site, the recovery of one proton by the probe, the changes in solvation by decane caused by the conversion of the acid and the base into the conjugated base and conjugated acid, and also all other enthalpic effects associated with the ion pairs which could be formed or broken during the neutralization reaction [31]. It can be seen in Fig. 6 that the Al-SBA-15 (Si/Al_{gel} = 8) sample manifests the lowest acidity (similar to aluminum-free SBA-15) while Al-SBA-15 (Si/Al_{gel} = 15) exhibits the highest acidity. It could be concluded that a more precise estimation of the acidity of Al-SBA-15 (Si/Al_{gel} = 8) requires a different solvent or probe. By the same argument, it could be noticed that the adsorption in decane causes an overestimation of the acidity of Al-SBA-15 (Si/Al_{gel} = 15) sample. These findings are in opposition with the results obtained in gas phase adsorption measurements, where both sets of experiments clearly show that Al-SBA-15 (Si/Al_{gel} = 8) is more acidic than Al-SBA-15 (Si/Al_{gel} = 15). Carniti et al. [30] have studied the influence of the solvent (toluene, decane and cyclohexane) on the adsorption of aniline and 2-ethyl-phenylamine on niobic acid and niobium phosphate. The heat evolved for aniline adsorption on niobic acid in toluene was nearly twice that released in decane. The measured heats were similar for the adsorption of aniline in toluene and cyclohexane on niobium phosphate but greater than in decane. These results emphasize the importance of the nature of the liquid dispersing phase and how particular solids are differently affected.

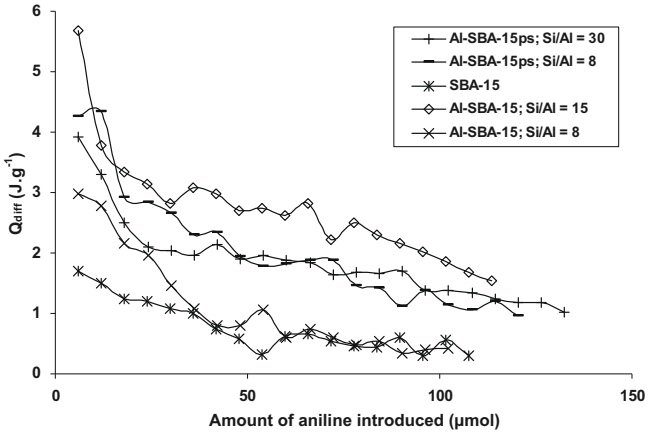

Fig. 6. Evolved heat for each dose of aniline as a function of the amount of probe sent onto the samples in *n*-decane.

The calorimetric data indicate the number, the strength and the strength distribution of the acid sites, and give some indications about the nature of these sites. Infrared spectroscopy of pyridine adsorption gives a more complete picture, making a better distinction between the two types of sites (Brönsted and Lewis); this makes it a good technique to complete the calorimetric results. Fig. 7(a–c) displays the spectra of pyridine desorption at different temperatures (25–400 °C) on Al-SBA-15 (Si/Al_{gel} = 8) (a), Al-SBA-15ps (Si/Al_{gel} = 30) (b) and Al-SBA-15ps (Si/Al_{gel} = 8) (c) after adsorption at room temperature on the pretreated wafers.

All spectra contain bands corresponding to υ_{CN} vibrations of pyridine which appear at

- 1545 cm^{-1} due to the formation of pyridinium ions (**PyH^+**) on Brönsted sites,
- 1490 cm^{-1} which is associated to pyridine adsorption on Brönsted and Lewis sites at the same time, and
- 1455 cm^{-1} characteristic of pyridine coordinated to a Lewis site (**PyL**).

The evolution of the intensity bands as a function of desorption temperature can offer information about the acid strength of the solids. Thus, the presence of these bands at high temperature is a sign of the high acid strength of the solids.

The band which appears at 1444 cm^{-1} is attributed to physisorbed pyridine. Above 100 °C, this band completely disappears, indicating that only chemisorbed pyridine remains on the solids. A phenomenon that it was observed for all three samples is a shift of the band at 1490 cm^{-1} to 1495 cm^{-1}, at temperatures above 300 °C. For Al-SBA-15 prepared by post-synthesis (b and c), the band at 1490 cm^{-1} is divided into two bands (1490 and 1495 cm^{-1}) at 300 °C. At 400 °C, only the band at 1495 cm^{-1} was observed. To our knowledge this band at 1495 cm^{-1} has not been reported in any previous studies of Al-SBA-15 samples. However, Vinh-Thang et al. have found this band when studying pyridine adsorption on micro-mesoporous UL-ZSM-5 materials [32,33]. The appearance of this band clearly shows the presence of two types of Lewis sites in Al-SBA-15 samples. Although the nature and mechanism of formation of these Lewis sites are still unclear, this kind of acidity could be generated by either extra framework aluminum species, such as AlO_5 and AlO_6, or defect sites such as AlO_3, or both. Depending on the synthesis and/or calcination conditions, one of these forms could predominate. The spectra of pyridine desorption at gradually increasing temperatures show that, at room temperature, octahedral aluminum identified by ^{27}Al NMR is responsible for the Lewis acidity [34]. Lewis sites in zeolites are also generated by tri-coordinated framework aluminum species, as well. Van Bokhoven et al. [34] proposed three mechanisms of formation of tri-coordinated aluminum species in zeolites. All these mechanisms occur at temperatures over 400 °C: (i) the breaking of the weakest Al-O bond without complete dehydroxylation (nevertheless, it is possible for this breaking to be followed by dehydroxylation, and in a subsequent step, extraction of aluminum from the framework may occur; extraction seems to depend on the aluminum position in the framework), (ii) a bridging hydroxyl group is dehydroxylized with a nearby Si-OH group, releasing

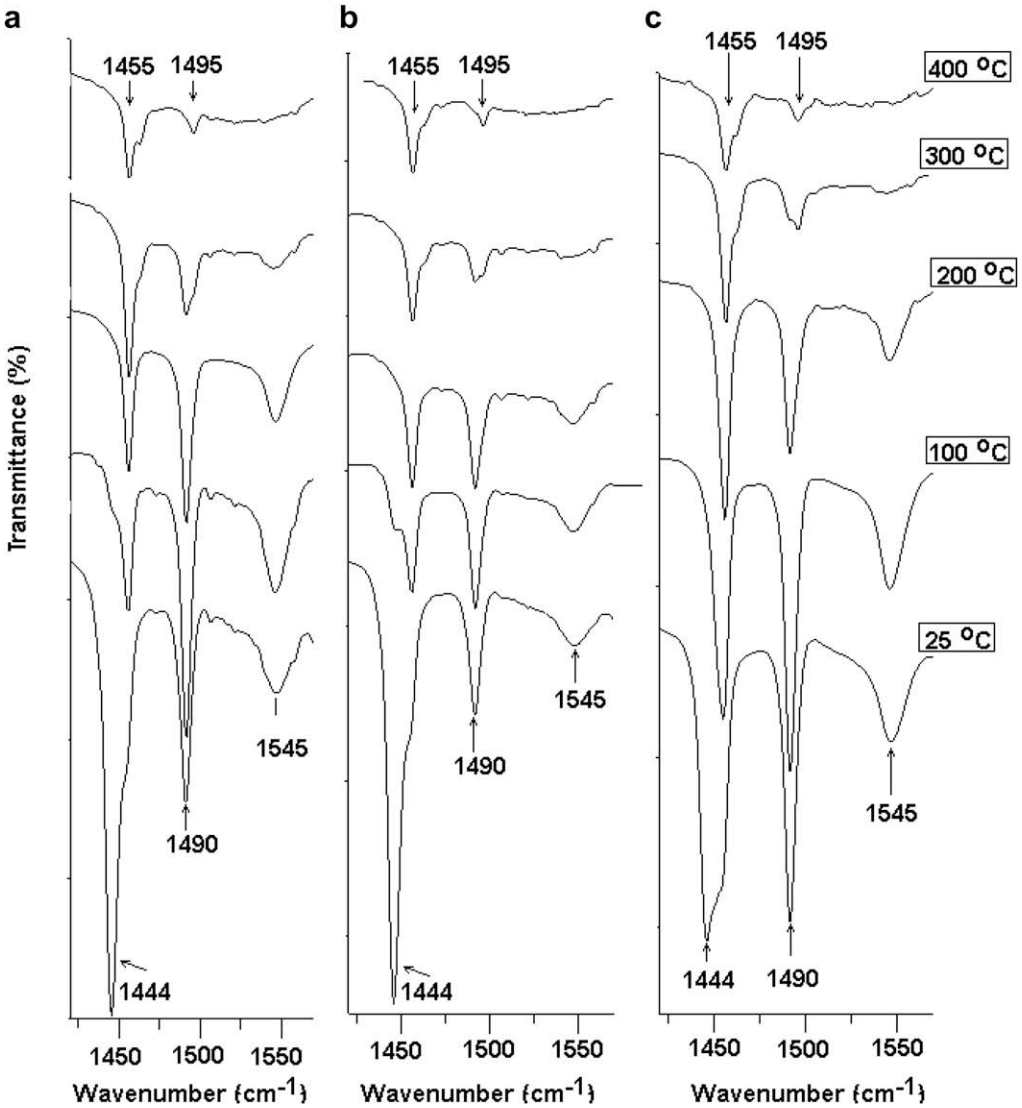

Fig. 7. FT-IR spectra of pyridine desorption on Al-SBA-15 (Si/Al_{gel} = 8) (a), Al-SBA-15 ps (Si/Al_{gel} = 30) (b) and Al-SBA-15 ps (Si/Al_{gel} = 8) (c) at different temperatures.

water, and (iii) a defect site on the aluminum atom causes the irreversible formation of AlO_3 species [34]. On the other hand, the formation of new Lewis sites observed only in the IR spectra for the grafted samples could indicate that the aluminum source is important, as well. The grafting of aluminum on mesoporous silica using aluminum chloride as aluminum precursor has been discussed in the literature [35,36]. Depending on the grafting conditions (humid atmosphere or moisture free conditions) different types of Lewis sites could be formed, as identified by ^{27}Al NMR [35]. In our case, the grafting as well as ^{27}Al NMR were performed under moisture conditions, while the IR spectra were collected after degassing at gradually increasing temperatures. This is the reason why our ^{27}Al NMR spectra show only the classical signal at 0 and 50 ppm whereas the IR spectra reveal supplementary Lewis sites. It may be assumed that starting from 300 °C the Lewis sites identified by the above-mentioned studies [35,36] could form in our samples and are responsible for the band at 1945 cm^{-1}.

XPS can be used to evaluate the ratio between the Brönsted and Lewis site populations, based on the variations of the binding energy of N1s according to the environment of the nitrogen atom after ammonia adsorption [37–40]. Because XPS analysis is performed under ultravacuum, the physically adsorbed molecules are desorbed and only the strongest adsorbed molecules are kept on the surface. Consequently, this technique can provide only the identification and a quantitative determination of the strongest Brönsted and Lewis sites, especially for the amorphous solids where the strength of sites is not comparable to that of zeolites.

Fig. 8 shows XP spectra for three of the Al-SBA-15 samples after NH_3 adsorption at 80 °C. The experiments were performed at this temperature in order to keep the same conditions as for the ammonia adsorption in gas phase calorimetry. The solids studied by XPS are Al-SBA-15 (Si/Al_{gel} = 8 and 15) obtained by direct synthesis and Al-SBA-15ps (Si/Al_{gel} = 8) prepared by post-synthesis.

According to the literature [41], when a basic molecule reacts with a Brönsted site, the binding energy of N1s is between 402–402.8 eV, while when it forms a complex with a Lewis site, the binding energy is between 399 and 401.5 eV. It can be seen in Fig. 8 that all three samples have both types of acid sites previously identified by infrared spectroscopy of pyridine desorption.

The N/Al ratios given in Table 3 can be used to compare the actual site concentration with the potential population of acid sites considering that, theoretically, each aluminum atom of the lattice can be at the origin of Brönsted or Lewis acidity. More precisely, the atomic N/Al ratios indicate the amounts of sites able to retain ammonia under ultravacuum conditions.

Table 3
XPS results after NH_3 adsorption on Al-SBA-15 samples.

XPS results	Sample		
	Al-SBA-15 (Si/Al = 8)	Al-SBA-15ps (Si/Al = 8)	Al-SBA-15 (Si/Al = 15)
N/Al (molar ratio)	0.72	0.46	0.92
% B/L	60/40	65/35	60/40

The results shown in this table illustrate that in ultravacuum conditions, the adsorbed ammonia covered only 72% of the "theoretical" acid sites in Al-SBA-15 (Si/Al_{gel} = 8), 46% in Al-SBA-15ps (Si/Al_{gel} = 8) and 92% in Al-SBA-15 (Si/Al_{gel} = 15). Therefore, Al-SBA-15ps (Si/Al_{gel} = 8) shows a much larger population of weak sites than Al-SBA-15 (Si/Al_{gel} = 8), while Al-SBA-15 (Si/Al_{gel} = 15) exhibits very few weak sites on its surface. On the other hand, Brönsted to Lewis ratios are comparable from one sample to another.

3.2. Adsorption studies

The adsorption potentials for removal of some volatile organic compounds (VOCs) such as methyl ethyl ketone (MEC), propionaldehyde (PAL) and acetonitrile (ACN) in gas phase have been probed for the mesoporous materials investigated in this work.

The uptake values obtained for MEC adsorption (Fig. 9) are in good agreement with data for nitrogen physisorption. As expected, SBA-15 presents the lowest adsorptive capacity. After aluminum incorporation by direct synthesis, the increased surface areas and pore volumes (Table 1) allow higher amounts of MEC to be retained on the sample surface. However, the amounts adsorbed are lower than in the data corresponding to nitrogen sorption. It can be seen that the adsorbed amounts of MEC are between 1400 and 2100 $\mu mol\ g^{-1}$, which correspond to 0.125 and 0.188 $cm^3\ g^{-1}$ respectively. Vinh-Thang et al. [42] observed the same behavior for toluene and n-heptane adsorptions on SBA-15. This observation could be explained by "lateral" sorbate-sorbate interactions, in which the first adsorbed molecules prevent subsequent sorbate molecules from getting as close to the surface, causing them to be less strongly adsorbed.

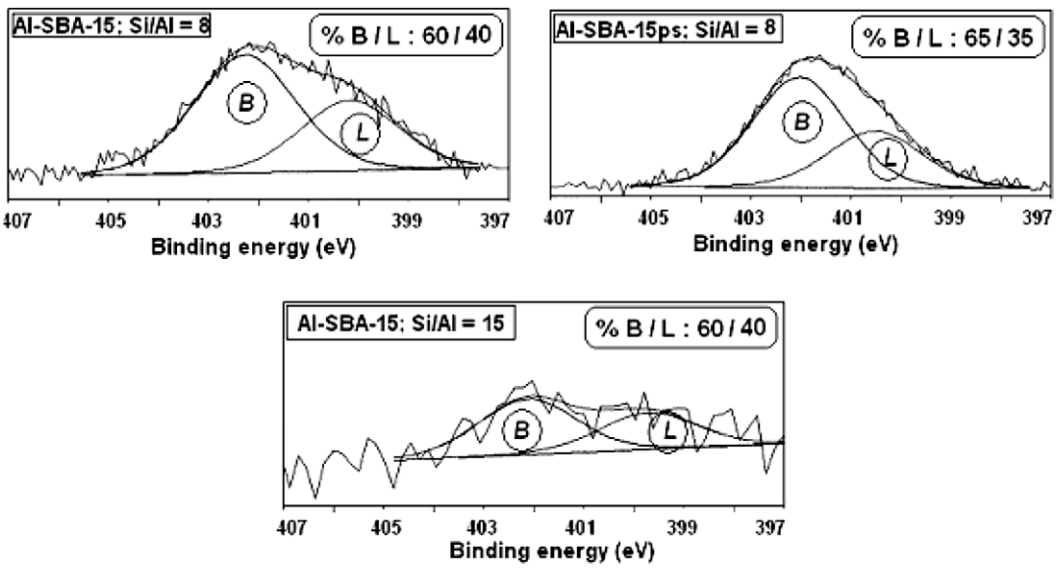

Fig. 8. N1s XP spectra after adsorption of NH_3 at 80 °C on three Al-SBA-15.

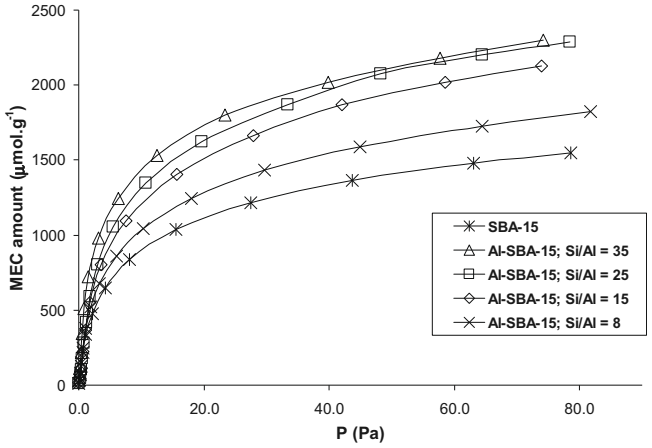

Fig. 9. Volumetric isotherms of MEC adsorption at 30 °C on SBA-15 and Al-SBA-15 direct-synthesis samples.

The volumetric isotherms for PAL adsorption are presented in Fig. 10 for Al-SBA-15 with Si/Al_{gel} = 15, 25 and 35 obtained by direct synthesis. The results are compared to those of aluminum-free SBA-15.

Although the volumetric isotherms show that the amounts of PAL adsorbed on Al-SBA-15 samples are quite similar, an improvement compared to SBA-15 can be noticed. However, for the sample with Si/Al_{gel} = 35 a different shape of the curve was observed. Correlating this result with the evolved heats (Supplementary material 3), the existence of small amounts of extra framework aluminum obstructing the pores can be conjectured, thus inducing some diffusion problems at the beginning of the adsorption and preventing the isotherm to follow the Langmuir profile anymore. As the amount of adsorbed aldehyde increases, the adsorption capacity seems to improve. The adsorption isotherm for Al-SBA-15 with Si/Al_{gel} = 8 is not represented here. According to the acidity studies, this sample contains both types of acid sites (Brönsted and Lewis). Recall that aldehydes very easily give rise to aldol condensation under mild reaction conditions. On the sample with Si/Al_{gel} = 8, the aldehyde molecules reacted with each other to form an aldol (2-hydroxy-butanal) starting around an equilibrium pressure of 13 Pa. Due to this unwanted reaction, we did not continue the experiment on this sample up to the final pressure of 67 Pa. However this behavior suggests that this sample might be a good catalyst for aldehyde condensation. Over aluminum-free SBA-15, whose acidity is generated only by surface silanol groups, PAL molecules adsorb *via* hydrogen bonds established between hydrogen of the silanol group and carbonylic oxygen. Concerning the adsorption of PAL on Al-SBA-15 (Si/Al_{gel} = 25), it seems that extra-framework aluminum distribution on the surface is such that it does not obstruct pores. Anyway, the amount of aluminum is low enough to prevent the reaction between PAL molecules, thus confirming the low acidity.

Fig. 11 presents the volumetric isotherms of acetonitrile adsorption on SBA-15 and Al-SBA-15 samples prepared by direct-synthesis and post-synthesis. The post-synthesis samples and one of the direct-synthesis samples (Al-SBA-15 (Si/Al_{gel} = 35) exhibit a different behavior compared to SBA-15 and the other Al-SBA-15 samples obtained by direct synthesis. It is obvious that at low coverage the adsorption is very poor on the three above-mentioned samples.

Correlating these results with those obtained for nitrogen sorption, it could be pointed out that in the case of the post-synthesis samples, the aluminum complexes obstructing the micropores could form Lewis sites, which interact with the first ACN molecules sent on the samples. Also, it could happen that part of the aluminum is located at the mouth of mesopores, blocking the entrance of the probe molecules into the channels. Trapped acetonitrile could also interact with this aluminum, leading to some diffusion problems. It is already known that acetonitrile adsorption is often affected by diffusion problems, and because of this it is recommended to increase the temperature of the adsorption [43]. An additional feature is the influence of the adsorption site environment. Gorte and White [44] have studied the adsorption of different molecules including acetonitrile on zeolites in order to show the influence of the environment of the Brönsted acid sites on catalytic activity. They found that the nature of the adsorption complexes is affected by the environment created by the zeolite cavities.

In order to compare the adsorption of the different VOCs, the volumetric isotherms as well as the evolved heats for the adsorption of all three pollutants (acetonitrile, propionaldehyde and methyl ethyl ketone) on pure SBA-15 are illustrated in Fig. 12. The stronger adsorbate-adsorbent interactions were observed for MEC molecules as confirmed by the heats of adsorption. As mentioned above (Supplementary material 2 and corresponding discussion), SBA-15 presents a heterogeneous distribution of adsorption sites. This situation could be explained in terms of hybridization and gas-phase basicity. Both the ketone and the aldehyde contain in the molecule a carbonyl group in which the oxygen is sp^2 hybridized. This oxygen is a base which can be attacked by an electrophile. The difference between PAL and MEC consists in the

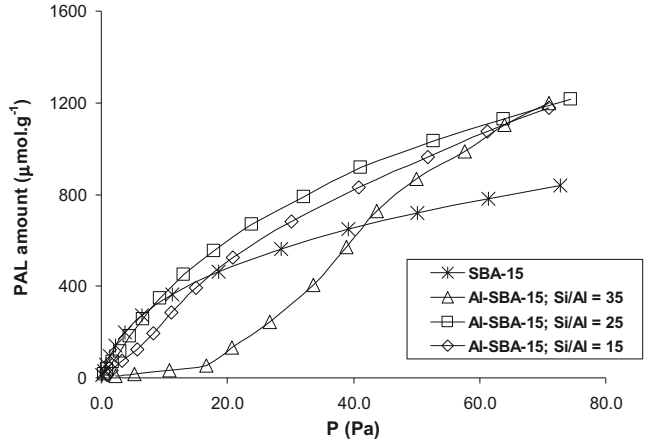

Fig. 10. Volumetric isotherms of PAL adsorption at 30 °C on SBA-15 and three of the Al-SBA-15 samples obtained by direct-synthesis.

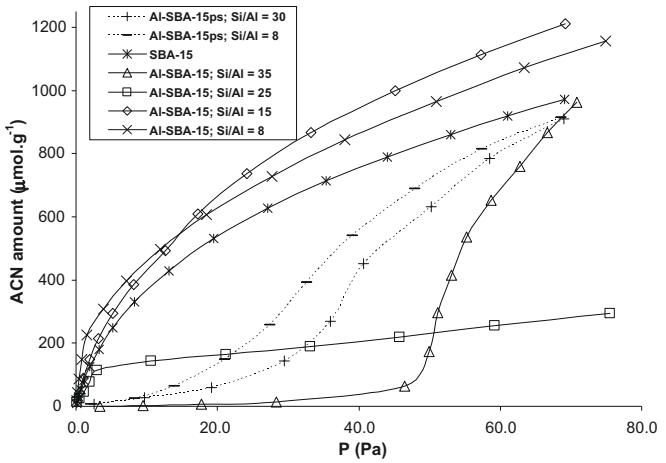

Fig. 11. Volumetric isotherms of ACN adsorption at 30 °C on SBA-15 and Al-SBA-15.

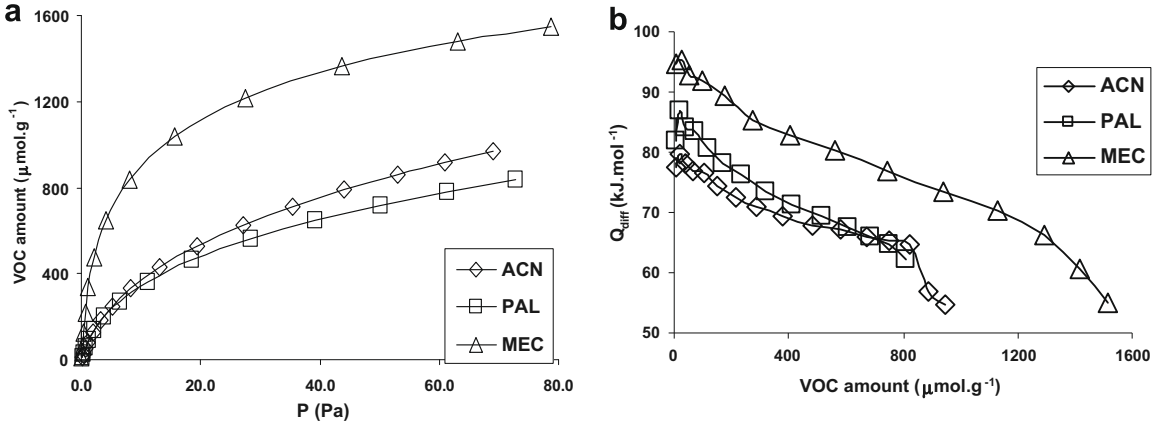

Fig. 12. Volumetric isotherms (left) and differential heats (right) of VOCs adsorptions at 30 °C on pure SBA-15.

presence of a methyl group bonded to the carbonylic carbon in methyl ethyl ketone. This group has a positive inductive effect which increases the density of electrons around the carbonylic oxygen raising the availability of the electron pair, so that it can more easily accept a proton. Therefore, this oxygen is more basic than that of the propionaldehyde. The proton affinities, which measure the basicity of the molecules in gas phase, sustain this explanation. Indeed, the proton affinity of MEC is 787.09 kJ mol^{-1} [45] while that of PAL is 781.66 kJ mol^{-1} [46]. Thus, the ketone has more affinity for the weakly acidic silanols present on the SBA-15 surface. It can be pointed out that more silanols are involved in this adsorption than for propionaldehyde. Acetonitrile adsorption on SBA-15 can also be analyzed in similar terms. The proton affinity of this molecule is 778.74 kJ mol^{-1} [45]. Moreover, cyano nitrogen has *sp* hybridization, which holds the electrons closer than an sp^2 hybridized atom, thus resulting in lower basicity for ACN [47]. Although the amount of ACN adsorbed is a little bit higher than for PAL, the interaction strength is weaker than for PAL.

The size and the shape of the molecules were considered in this study, as well. The critical diameter of ACN can be taken as similar to that of methane (0.40 nm) or of ethane (0.44 nm) [48], while MEC has a kinetic diameter of 0.57 nm [49]. As ACN is the smallest molecule, this molecule should be better adsorbed than the other two molecules. However, the curves of the evolved heats and the adsorption isotherms show a higher capacity of adsorption and a stronger adsorption for MEC molecule, while ACN was the poorest adsorbed molecule on the SBA-15 surface. Therefore, these findings point out the reduced influence of the size and molecular shape of the molecules on the adsorption.

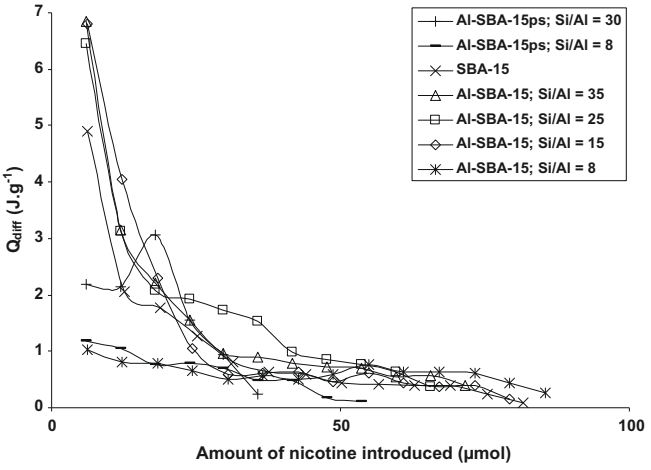

Fig. 13. Evolved heat for each dose of nicotine as a function of the amount of probe molecule sent onto the samples.

Fig. 13 shows the evolved heats *vs.* the amount of nicotine sent for adsorption on Al-SBA-15 samples obtained by direct and post-synthesis. The results are compared to those obtained for nicotine adsorption on SBA-15.

Depending on the surface characteristics, different behaviors are observed, falling into two categories. For the first injected doses, purely siliceous SBA-15 and Al-SBA-15 samples with low aluminum content (such as Al-SBA-15 (Si/Al_{gel} = 15, 25, 35)) exhibit practically the same behavior. The evolved heats are high (5–7 J g^{-1}). The adsorption sites are progressively covered by nicotine, so that the heats gradually decrease until 0.5 J g^{-1}. It can be observed that the decrease in evolved heat is very fast for SBA-15, while for Al-SBA-15 the evolved heats decrease more slowly.

On the other side, for Al-SBA-15 samples rich in aluminum (the post-synthesis samples and Al-SBA-15 (Si/Al_{gel} = 8) prepared by direct-synthesis), the evolved heats are low (1–2 J g^{-1}) for the first injected doses.

These two different tendencies could indicate that aluminum may increase the affinity of the adsorbent for water, thus diminishing its affinity for the organic molecule.

The adsorption of nicotine in liquid phase depends on different factors. First of all, the basicity and conformation of nicotine in liquid phase are different from those in gas phase [50–52]. Secondly, the Brönsted sites of the post-synthesis samples and Al-SBA-15 (Si/Al_{gel} = 8) obtained by direct-synthesis are in dissociated form. It is important to keep in mind that, although we are considering Brönsted sites in a mesoporous material, their strength is not comparable to that of the sites present in zeolites. On the other hand, silanol groups are not acidic enough to adsorb nicotine *via* a neutralization reaction. It is more plausible that there are electrostatic attractions between the aromatic ring of nicotine and the oxygen of dissociated silanol groups. The affinity of the adsorbent for the probe molecule is reflected by the evolved heats. As the affinity increases, the evolved heat increases and the thermal balance shifts in favor of the contribution of the adsorption effects.

4. Conclusion

In this paper, Al-SBA-15 mesoporous aluminosilicates with different Si/Al ratios between 8 and 35 were synthesized by both the direct-synthesis and post-synthesis methods. XRD and N_2 adsorption–desorption isotherms confirm that the specific mesoporous structure of SBA-15 is maintained whatever the pathway used. Incorporation of aluminum was successful for the samples ob-

tained by post-synthesis, and only for one sample synthesized by the direct method. Aluminum was mainly in tetrahedral coordination and only a small amount in octahedral coordination according to the ^{27}Al NMR measurements. Moreover, the synthesis path has influenced the textural properties of the solids. Direct synthesis favored the microporosity formation and led to higher surface area in comparison to SBA-15. On the other hand, post-synthesis method led to smaller surface area and micropores blocking. The acidic properties of the Al-SBA-15 samples were investigated by different techniques: ammonia and pyridine adsorption in gas phase microcalorimetry linked to a volumetric line, aniline adsorption in decane in liquid phase, infrared spectroscopy of pyridine adsorption, and XPS of ammonia adsorption, in order to obtain a complete picture of the acidity of the samples. The acidic properties of Al-SBA-15 were found to be improved in comparison to SBA-15, and they were correlated to Al content. Also, the synthesis method had significant influence on the acidity of samples. Post-synthesis samples exhibited higher acidity compared to the samples obtained by direct synthesis. Studies of the adsorptive capacities of SBA-15 mesoporous solids using organic pollutants belonging to three different groups, namely aldehydes (propionaldehyde), ketones (methylethylketone) and nitriles (acetonitrile) have shown that whatever the adsorbent, methylethylketone was better retained than the other pollutants. The chemistry of the adsorbed molecules, hybridization and gas-phase basicity had more importance than their shape or size during adsorption. An alkaloid (nicotine) was adsorbed in water in order to check the influence of aluminum on the adsorption capacity of the sample. We have shown that the aluminum content strongly influenced the competition between adsorbate and solvent during adsorption onto the solid surface.

References

[1] J.D. Sherman, Proc. Natl. Acad. Sci. USA 96 (1999) 3471.
[2] F. Rouquerol, J. Rouquerol, K. Sing, Adsorption by Powders and Porous Solids: Principles, Methodology and Applications, Academic Press, London, 1999.
[3] D. Zhao, J. Feng, Q. Huo, N. Melosh, G.H. Fredrickson, B.F. Chmelka, G.D. Stucky, Science 279 (1998) 548.
[4] M. Trombetta, G. Busca, M. Lenarda, L. Storaro, M. Pavan, Appl. Catal. A: General 182 (1999) 225.
[5] A. Vinu, V. Murugesan, W. Böhlmann, M. Hartmann, J. Phys. Chem. B 108 (2004) 11496.
[6] A. Vinu, D.P. Sawant, K. Ariga, V. Hartmann, S.B. Halligudi, Micropor. Mesopor. Mater. 80 (2005) 195.
[7] H.-M. Kao, C.-C. Ting, S.-W. Chao, J. Molec. Catal. A: Chem. 235 (2005) 200.
[8] S. Zeng, J. Blanchard, M. Breysse, Y. Shi, X. Shu, H. Nie, D. Li, Micropor. Mesopor. Mater. 85 (2005) 297.
[9] Z. Luan, M. Hartmann, D. Zhao, W. Zhou, L. Kevan, Chem. Mater. 11 (1999) 1621.
[10] Y. Li, W. Zhang, L. Zhang, Q. Yang, Z. Wei, Z. Feng, C. Li, J. Phys. Chem. B 108 (2004) 9739.
[11] G.J.A.A. Soler-Illia, E.L. Crepaldi, D. Grosso, C. Sanchez, Curr. Opin. Colloid Interface Sci. 8 (2003) 109.
[12] R. Mokaya, W. Jones, J. Mater. Chem. 9 (1999) 555.
[13] R. Mokaya, W. Jones, Chem. Commun. (1998) 1839.
[14] J.J. Chiu, D.J. Pine, S.T. Bishop, B.F. Chmelka, J. Catal. 221 (2004) 400.
[15] Y. Oumi, H. Takagi, S. Sumiya, R. Mizuno, T. Uozumi, T. Sano, Micropor. Mesopor. Mater. 44–45 (2001) 267.
[16] S. Sumiya, Y. Oumi, T. Uozumi, T. Sano, J. Mater. Chem. 11 (2001) 1111.
[17] S.C. Shen, S. Kawi, J. Phys. Chem. 103 (1999) 8870.
[18] W.W. Lukens Jr., P. Schmidt-Winkel, D. Zhao, J. Feng, G.D. Stucky, Langmuir 15 (1999) 5403.
[19] M. Hartmann, A. Vinu, Langmuir 18 (2002) 8010.
[20] V.-T. Hoang, Q. Huang, M. Eic, D. Trong-On, S. Kaliaguine, Langmuir 21 (2005) 2051.
[21] C.G. Sonwane, P.J. Ludovice, J. Molec. Catal. A: Chem. 238 (2005) 135.
[22] G. Leofanti, M. Padovan, G. Tozzola, B. Venturelli, Catal. Today 41 (1998) 207.
[23] M. Kruk, V. Antochshuk, M. Jaroniec, A. Sayari, J. Phys. Chem. B 103 (1999) 10670.
[24] Y.-S. Ooi, R. Zakaria, A.R. Mohamed, S. Bhatia, Catal. Commun. 5 (2004) 441.
[25] G. Engelhardt, D. Michel, High-Resolution Solid-Dtate NMR of Silicates and Zeolites, John Wiley and Sons Ltd., 1987.
[26] A. Auroux, Top. Catal. 4 (1997) 71. 19 (2002) 205.
[27] A. Auroux, Acidity and Basicity: Determination by Adsorption Microcalorimetry, Molecular Sieves, vol. 6, Springer-Verlag, Berlin, 2008.
[28] C. Lee, D.J. Parrillo, R.J. Gorte, W.E. Farneth, J. Am. Chem. Soc. 118 (1996) 3262.
[29] R.S. Drago, S.C. Dias, M. Torrealba, L. de Lima, J. Am. Chem. Soc. 119 (1997) 4444.
[30] P. Carniti, A. Gervasini, S. Bennici, J. Phys. Chem. B 109 (2005) 1528.
[31] S. Koujout, D.R. Brown, Catal. Lett. 98 (2004) 195.
[32] H. Vinh-Thang, Q. Huang, A. Ungureanu, M. Eic, D. Trong-On, S. Kaliaguine, Langmuir 22 (2006) 4777.
[33] H. Vinh-Thang, Q. Huang, A. Ungureanu, M. Eic, D. Trong-On, S. Kaliaguine, Micropor. Mesopor. Mater. 92 (2006) 117.
[34] J.A. van Bokhoven, A.M.J. van der Eerden, D.C. Koningsberger, J. Am. Chem. Soc. 125 (2003) 7435.
[35] S. Sato, G.E. Maciel, J. Molec. Catal. A: Chem. 101 (1995) 153.
[36] D. Dube, S. Royer, D. Trong On, F. Beland, S. Kaliaguine, Micropor. Mesopor. Mater. 79 (2005) 137.
[37] R.B. Borade, A. Adnot, S. Kaliaguine, J. Chem. Soc. Faraday Trans. 86 (1990) 3949.
[38] M. Huang, A. Adnot, S. Kaliaguine, J. Am. Chem. Soc. 114 (1992) 10005.
[39] C. Guimon, A. Gervasini, A. Auroux, J. Phys. Chem. B 105 (2001) 10316.
[40] A. Auroux, A. Gervasini, C. Guimon, J. Phys. Chem. B 103 (1999) 7195.
[41] A. Boréave, A. Auroux, C. Guimon, Micropor. Mater. 11 (1997) 275.
[42] H. Vinh-Thang, Q. Huang, M. Eic, D. Trong-On, S. Kaliaguine, Langmuir 21 (2005) 5094.
[43] L. Yang, K. Trafford, O. Kresnawahjuesa, J. Sÿepa, R.J. Gorte, J. Phys. Chem. B 105 (2001) 1935.
[44] R.J. Gorte, D. White, Micropor. Mesopor. Mater. 447-455 (2000) 35.
[45] E.P. Hunter, S.G. Lias, J. Phys. Chem. Ref. Data 27 (1998) 413.
[46] R. Yamdagni, P. Kebarle, J. Am. Chem. Soc. 98 (1976) 1320.
[47] F. Ijjaali, O. Mo, M. Yanez, J-L.M. Abboud, J. Molec. Struct. (Theochem) 338 (1995) 225.
[48] M. Bevilacqua, A.G. Alejandre, C. Resini, M. Casagrande, J. Ramirez, G. Busca, Phys. Chem. Chem. Phys. 4 (2002) 4575.
[49] S.-C. Huang. Master's Thesis – Volumetric Measurement of the Adsorption Equilibrium of VOCs and Compared with the Gravimetric Measurement, 2006.
[50] A. de Lucas, P. Canizares, M.A. Garcia, J. Gomez, J.F. Rodriguez, Ind. Eng. Chem. Res. 37 (1998) 4783.
[51] J.F. Pankow, A.D. Tavakoli, W. Luo, L.M. Isabelle, Chem. Res. Toxicol. 16 (2003) 1014.
[52] D.E. Elmore, D.A. Dougherty, J. Org. Chem. 65 (2000) 742.